MRS Communications (2017), 7, 785–797
© Materials Research Society, 2017
doi:10.1557/mrc.2017.116

MRS Communications

Prospective Article

Recent progress in the concurrent atomistic-continuum method and its application in phonon transport

Xiang Chen, Weixuan Li, Adrian Diaz, Yang Li, and **Youping Chen,** Department of Mechanical and Aerospace Engineering, University of Florida, Gainesville, Florida 32611, USA
David L. McDowell, Woodruff School of Mechanical Engineering, Georgia Institute of Technology, Atlanta, Georgia 30332, USA; School of Materials Science and Engineering, Georgia Institute of Technology, Atlanta, Georgia 30332, USA
Address all correspondence to Xiang Chen at **xiangchen@ufl.edu**

(Received 25 July 2017; accepted 10 October 2017)

Abstract

This work presents the recent progress in the development of the concurrent atomistic-continuum (CAC) method for coarse-grained space- and time-resolved atomistic simulations of phonon transport. Application examples, including heat pulses propagating across grain boundaries and phase interfaces, as well as the interactions between phonons and moving dislocations, are provided to demonstrate the capabilities of CAC. The simulation results provide visual evidence and reveal the underlying physics of a variety of phenomena, including phonon focusing, wave interference, dislocation drag, interfacial Kapitza resistance caused by quasi-ballistic phonon transport, etc. A new method to quantify fluxes in transient transport processes is also introduced.

Introduction

Thermal transport has been studied for over 200 years. However, the strong interest in its micro/nanoscale details did not emerge until the late 1980s. The last decade has witnessed a remarkable focus on ever-decreasing scales, with modeling and simulation playing a significant role. Unfortunately, due to the limited computational resources, it is still challenging to move up from the atomic and nanoscale to model phonon interactions with mesoscale defect structures in lattices. It remains an inherently multiscale computational challenge.[1]

After decades of development, there are several computational tools for phonon transport that have provided the community with very useful insight. As one of the pioneering methods in simulating phonon transport, the Boltzmann transport equation (BTE), with the help of recently developed efficient Monte Carlo algorithms, has been extended for the study of mesoscale material systems.[2,3] In BTE, the defects are not resolved in realistic simulation domains, but are considered indirectly through the extrinsic relaxation time of phonons. The relaxation time, together with other information regarding phonons, then needs to be obtained from either phenomenologic models or other methods at lower length scale such as the first-principles approach based on the density functional theory (DFT), the molecular dynamics (MD) simulation, or the atomistic Green's function (AGF) method. However, these methods currently cannot realistically represent irregular defect structures that extend to the mesoscale, e.g., incoherent grain boundaries (GBs), multiple defects, moving dislocations, etc. Simulating phonon interfacial transport and phonon-dislocation interactions have been recently identified as some of the most significant challenges in this field. The difficulty lies in "incorporating defects in realistic simulation domains,"[4] both spatially and temporally. To achieve this, "we need to connect transport simulation to structural simulations,"[4] as stated by Chen. Moreover, in BTE, the effects of different defects are simply combined via Mathiessen's rule, which means the scattering mechanisms of multiple defects, as well as the intrinsic phonon–phonon scattering, are all assumed to be independent of each other. In addition, the BTE technique treats phonons as particles; this makes it inappropriate for the study of wave effects, i.e., wave interference.[4] For the study of phonon transport across an interface, the AGF method pioneered by Mingo and Yang[5] emerged a decade ago and has demonstrated its potential. Similar to the lattice dynamics (LD) method, the AGF technique is a frequency domain method ideally suited for phonon mode analysis and frequency-specific transmission across interfaces. However, in AGF and LD, interfaces are treated as a time-invariant input. This means that they only consider the effect of defects on phonon transport, with the possible evolution of interfacial structures being ignored. In addition, the AGF and LD are based on the harmonic force constants from an empirical model or DFT calculations; the inclusion of anharmonicity, although possible in principle, requires significantly more effort and is not generally pursued in the literature[6].

To model phonon transport in materials with defects, MD is essentially the only tool presently available that does not require

https://doi.org/10.1557/mrc.2017.116 Published online by Cambridge University Press

assumptions regarding the nature of phonon transport or a preconceived understanding of phonon-defect scattering.[7,8] Equilibrium MD with the Green–Kubo algorithm can be used to compute thermal conductivity and, if projected onto harmonic normal modes, it can be used for a modal analysis.[9] However, since it assumes one heat flux for the entire specimen, the method is only appropriate for the homogeneous material system.[10] The non-equilibrium steady-state MD is analogous to the quasi one-dimensional (1D) steady-state experiment and is straightforward in terms of data analysis. One component of the thermal conductivity tensor can be obtained in each simulation by fitting the temperature profile to Fourier's law.[11–13] MD can also be used to simulate transient transport processes, such as heat pulse propagation, if the heat pulse is properly modeled. The major limitation of using MD for the study of phonon-defect interaction is the size limit. The maximum phonon wavelength that can be considered in the simulation is the length of the MD simulation cell. Thus, the effect of long-wavelength phonons cannot be investigated. However, phonon transport in short-period superlattices, e.g., has experimentally been shown to be dominated by long-wavelength phonons.[14] Even for single-crystalline Si at room temperature, phonons with micron-sized wavelength contribute more than 40% of the thermal conductivity.[15] In addition, phonon interactions with microstructures, including their dynamic evolution, that extends to a higher length scale in space cannot be modeled with a simulation cell that is not sufficiently large.

Therefore, existing methodologies for simulating phonon transport, such as the BTE and the AGF methods, cannot be used to predict the dynamic evolution of the microstructures that undergo reconstruction in response to phonon scattering. Although MD simulations can address such phenomena in principle, they are limited to accessing relatively small length scales in describing phonon-defect interactions. The objective of this work is to introduce and demonstrate recent progress in the fully dynamic concurrent atomistic-continuum (CAC) method, which has potential to meet the needs for space- and time-resolved simulation of highly non-equilibrium transport processes in materials in a manner coupled with evolution of defect structures at extended scale, addressing mesoscale phenomena beyond the length scale limitations typical of MD.

The rest of the article is organized as follows. The CAC methodology for simulation of phonon transport is presented in The CAC method section, including verifications of the method in predicting phonon dynamics. In the Verification of CAC in simulating phonon transport section, we present three numerical examples to demonstrate the capabilities of CAC in simulating ballistic and diffusive phonon propagation, their interaction with defects, as well as the dynamic responses of the defects. In the CAC simulations of coupled phonon transport and defect dynamics section, we present atomistic formula for heat flux that can be used to compute heat flux in transient processes and inhomogeneous systems. This paper is concluded with a brief summary and discussion in the Summary and discussions section.

The CAC method

A brief introduction

The CAC method is a coarse-grained atomistic method that reduces the degrees of freedom of an atomistic system by reformulating the continuum field representation of balance laws from the atomistic model.[16] We emphasize here its fully dynamic form. The theoretical foundation of the CAC method includes a coarse-graining concept based on the two-level description of crystals in solid-state physics and a unified atomistic–continuum formulation of the conservation laws based on the principles of classical statistical mechanics. The solid-state physics and statistical mechanics considerations can be summarized as follows.

(1) Solid-state physics describes the structure of all crystals in terms of a periodic lattice with a basis of atoms attached to each lattice point[17] (see Fig. 1). As the size of the lattice increases, the mechanical response associated with the structure becomes continuous.[18] CAC makes use of the translational symmetry of the crystal lattice and the lattice-level continuous properties to reduce the degrees of freedom of the atomistic model of crystalline materials. In contrast to many existing multiscale methods that coarse grain the atomic-scale structure or displacements, CAC reduces the degrees of freedom by assuming continuous deformation of the lattice while retaining information regarding discontinuous atomistic structure and response within any given unit cell in the case of polyatomic unit cells.

(2) Statistical mechanics has been the major theoretical tool to formulate a coarse-grained description of the microscopic dynamics of particles. For non-equilibrium systems, most

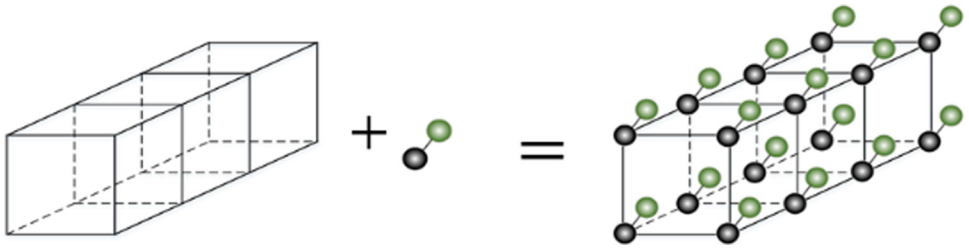


Figure 1. Solid-state physics description: "crystal structure = lattice + basis."[19]

https://doi.org/10.1557/mrc.2017.116 Published online by Cambridge University Press

developments have followed the work of Kirkwood on the "statistical mechanical theory of transport processes."[20,21] In 1950, Irving and Kirkwood formulated the hydrodynamics balance equations based on a molecular model, in which a continuum field description of local densities, such as stress and heat flux, is linked to the mass, position, and momentum of molecules, with the internal degrees of freedom within a molecule being ignored. In the first of a series of 14 classic papers, Kirkwood envisioned the extension of his formulation to molecules possessing internal degrees of freedom.[21] The CAC formulation is such an extension to the description of crystalline materials. It describes a crystalline material as a continuous collection of lattice cells with a group of discrete atoms embedded within each lattice cell.

This two-level description is motivated by Kirkwood's idea of including the internal molecular degrees of freedom,[21] the "lattice + basis" description of crystals in solid-state physics,[19] and also the two-level materials description in micromorphic theory.[22–27] Following the Irving–Kirkwood procedure,[20] this concurrent two-level description leads to a CAC representation of the conservation laws as exact consequences of Newton's second law,[28–30] i.e.,

$$\begin{aligned}
&\frac{d\rho^{\alpha}}{dt}+\rho^{\alpha}(\nabla_{\boldsymbol{x}}\cdot\boldsymbol{v}+\nabla_{\boldsymbol{y}^{\alpha}}\cdot\Delta\boldsymbol{v}^{\alpha})=0,\\
&\rho^{\alpha}\frac{d}{dt}(\boldsymbol{v}+\Delta\boldsymbol{v}^{\alpha})=\nabla_{\boldsymbol{x}}\cdot\boldsymbol{t}^{\alpha}+\nabla_{\boldsymbol{y}^{\alpha}}\cdot\boldsymbol{\tau}^{\alpha}+\boldsymbol{f}^{\alpha}_{\mathrm{ext}},\\
&\rho^{\alpha}\frac{de^{\alpha}}{dt}=\nabla_{\boldsymbol{x}}\cdot\boldsymbol{q}^{\alpha}+\nabla_{\boldsymbol{y}^{\alpha}}\cdot\boldsymbol{j}^{\alpha}+\boldsymbol{t}^{\alpha}:\nabla_{\boldsymbol{x}}(\boldsymbol{v}+\Delta\boldsymbol{v}^{\alpha})\\
&\qquad\qquad+\boldsymbol{\tau}^{\alpha}:\nabla_{\boldsymbol{y}^{\alpha}}(\boldsymbol{v}+\Delta\boldsymbol{v}^{\alpha}),
\end{aligned}\tag{1}$$

where $\boldsymbol{x}$ is the physical space coordinate of the continuously distributed lattice; $\boldsymbol{y}^{\alpha}$ ($\alpha=1, 2, \ldots, N_{\alpha}$, where N_{α} is the total number of atoms in a unit cell) is the subscale internal variable describing the position of atom relative to the mass center of the lattice located at $\boldsymbol{x}$; ρ^{α}, $\rho^{\alpha}(\boldsymbol{v}+\Delta\boldsymbol{v}^{\alpha})$, and $\rho^{\alpha}e^{\alpha}$ are the local densities of mass, linear momentum, and total energy, respectively; $\boldsymbol{v}+\Delta\boldsymbol{v}^{\alpha}$ is the atomic-level velocity and $\boldsymbol{v}$ is the velocity field; $\boldsymbol{f}^{\alpha}_{\mathrm{ext}}$ is the external force field; $\boldsymbol{t}^{\alpha}$ and $\boldsymbol{q}^{\alpha}$ are the momentum flux and heat flux due to the homogeneous deformation of lattice cells; $\boldsymbol{\tau}^{\alpha}$ and $\boldsymbol{j}^{\alpha}$ are the momentum flux and heat flux resulted from the reorganizations of atoms within the lattice cells. Solutions of the new conservation equations, supplemented by the underlying interatomic potential, provide both the continuous lattice deformation and the rearrangement of atoms within the lattice cells, thus leading to a CAC methodology; in the two limiting cases, namely the atomic and the macroscopic scales, the atomistic and continuum descriptions of transport processes are recovered.

CAC is also a continuum field theory since it treats a crystalline material as a continuous collection of material points (unit cells) that possess internal degrees of freedom to describe the movement of atoms inside each unit cell. In distinction from the two-level continuum description in micromorphic theory or other generalized continuum theories,[31,32] in CAC the subscale description within each continuously distributed material point is discrete, with atoms in each lattice cell being modeled explicitly. This complete set of governing equations governs both the atomistic and continuum regions, with the atomic-scale structure and interactions being built in the formulation. Different from the Irving and Kirkwood's statistical mechanics formulation of single-phase, single-component hydrodynamics equations, CAC employs a concurrent two-level structural description of materials. Therefore, CAC is unique in a number of regards:

(1) With a single precisely formulated set of conservation equations governing both atomic and continuum domains, the usual artificial interface between atomistic and continuum descriptions that limits most multiscale methods to consider only static phenomena is not needed.
(2) By including the internal degrees of freedom of atoms within each lattice cell in the continuum formulation, CAC can simulate complex crystalline materials, including both acoustic and optical phonon branches.
(3) With a complete field representation of the governing laws, the CAC formulation can be solved efficiently using continuum field simulation approaches, e.g., the finite element method. With the only constitutive relation being the interatomic potential and with a recast form of the governing equations, continuity between elements is not required; consequently, nucleation and propagation of dislocations or cracks can be simulated via sliding and separation between finite elements, as direct consequences of the governing equations.

Since CAC is derived solely from an atomistic model, it does not require continuum parameters for static, dynamic, zero, or finite temperature systems. In the process of the derivation, the fluxes are determined in terms of atomic displacements and local temperature. The CAC formulation is currently numerically implemented using a modified finite element method. It differs from traditional finite element implementations of classical continuum mechanics since each finite element in CAC represents a collection of continuously deformable primitive unit cells, each containing a group of atoms. Applications of CAC for the simulation of mechanical behavior have been demonstrated through the reproduction of dynamic phenomena such as crack propagation and branching,[33–35] phase transitions,[36] nucleation of dislocations, the formation of dislocation loops and networks,[37–43] and defect–interface interactions.[44]

Extending the form and capability of CAC to phonon transport

A recent development of CAC is to model coupled phonon dynamics and defect dynamics for non-equilibrium transient processes in heterogeneous materials. A motivation of this work is the recent advances in conducting transient experiments with direct photoexcitation that have led to observations

https://doi.org/10.1557/mrc.2017.116 Published online by Cambridge University Press

of many new phenomena, while improving the understanding of the underlying physics.[45–52] Especially at mesoscale, the experimental studies of phonon transport are dominated by this type of transient study. However, the majority of the existing MD studies are based on equilibrium and steady-state measurements.

To enable CAC to simulate heat pulse experiments, first, we have developed a phonon representation of heat pulses that are composed of spatiotemporal Gaussian wave packets, termed the coherent phonon pulse (CPP) model.[53] The CPP model is used to mimic the coherent excitation of a non-equilibrium phonon population achieved via ultrashort laser techniques. Since the CAC method is a coarse-grained method derived bottom–up from atomistics, and can adapt the viewpoint of phonons to describe heat and temperature in terms of mechanical vibrations, the CPP model naturally accommodates to the framework of CAC. In addition, since CAC is built on the statistical mechanical theory of transport processes of Irving–Kirkwood,[20,21] it can naturally be used to study highly non-equilibrium dynamic phonon transport processes. We believe that the capability of simulating the transient transport processes, together with the coarse-graining strategy in CAC that facilitates access to mesoscale defect structures and microstructures, moves these simulations closer to making contact with actual laboratory experiments and associated measured phenomena.

The current CAC method can be used for coarse-grained study of long-wavelength phonon dynamics and the dynamic interaction between phonons and defects. The propagation of heat pulses or defects, including their propagation directions and speeds, all emerge naturally in the simulation without the need for ballistic diffusive transport assumptions, or a priori understanding of the mechanism of phonon–phonon and phonon–defect interactions.

Verification of CAC in simulating phonon transport

Phonon dispersion relations

For the purpose of verification, we perform the LD calculation of the phonon dispersion relations for a 2D FCC solid with a Lennard–Jones (LJ) interatomic force field[54] and compare the results to the dispersions in CAC obtained by solving the dynamical matrix of the coarse-grained lattices. Figure 2 presents the frequency–wavelength relations along the [110] direction of the FCC crystal, containing both longitudinal acoustic (LA) and transverse acoustic (TA) branches. It is seen that the phonon dynamics predicted by CAC match the LD solution well within the range of the allowable wavelength. Here, the allowable wavelength (10 nm to 1 μm) is determined by the sizes of the specimen and the finite element mesh with an allowed error (<5%). The characteristic length of the specimen is ~1 μm, and the finite element contains eight unit cells along each direction. The calculation shows that CAC can reproduce the exact dynamics of an atomistic system if modeled with the finest mesh. When discretized with coarse-scale finite elements, CAC can accurately predict the dynamics of phonons with wavelengths longer than a critical wavelength determined by the size of the element.

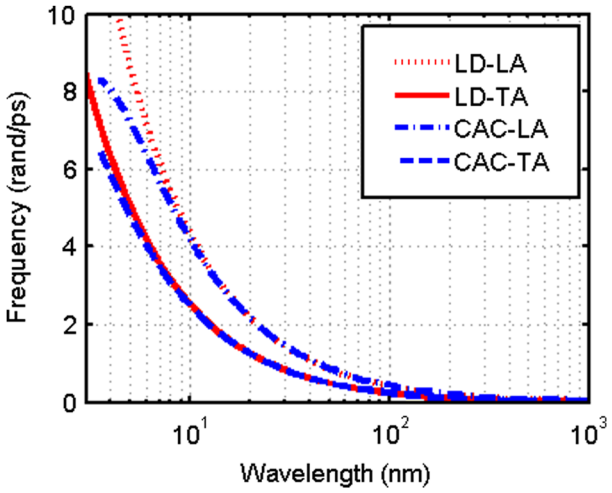


Figure 2. Phonon dispersion relations along the [110] direction within the (111) plane of a FCC crystal. The solutions calculated for the coarse-grained lattices in CAC (in blue) are compared with the lattice dynamics solution (in red).

Monochromatic wave propagation

Motivated by the experimental observations of radial phonon distributions in materials induced by the photoexcitation,[45] most of the numerical examples presented in this work are based on a point heat source propagation in a 2D computer model. In this section, we verify the simulation tool by considering the propagation of a continuous monochromatic radial wave (20 nm in wavelength) in a 2D model, and comparing the simulation results with MD. As can be seen in Fig. 3, when the mesh size approaches full atomic resolution, the CAC simulation with fine mesh generates the same results as MD. Note that the limited specimen size in the middle and for right columns induces surface reflection. With coarse graining, a larger computer model is simulated, and the exploded view of the same region around the heat source is presented in the left column for comparison. It is seen that the phonon wavelength, group velocity, and the slight hexagonal shape of wave crests caused by phonon focusing are reproduced by CAC with a coarse mesh in agreement with MD results.

Passing long-wavelength phonons through the numerical interfaces

To verify that there is no spurious wave reflection at the atomistic–continuum interface for the long-wavelength phonon propagation, the single-crystal model is discretized with both uniform meshes and non-uniform meshes, i.e., with both coarse meshes and fully atomistically resolved meshes. The CAC simulation is then conducted along with a CPP model,[53] which

https://doi.org/10.1557/mrc.2017.116 Published online by Cambridge University Press

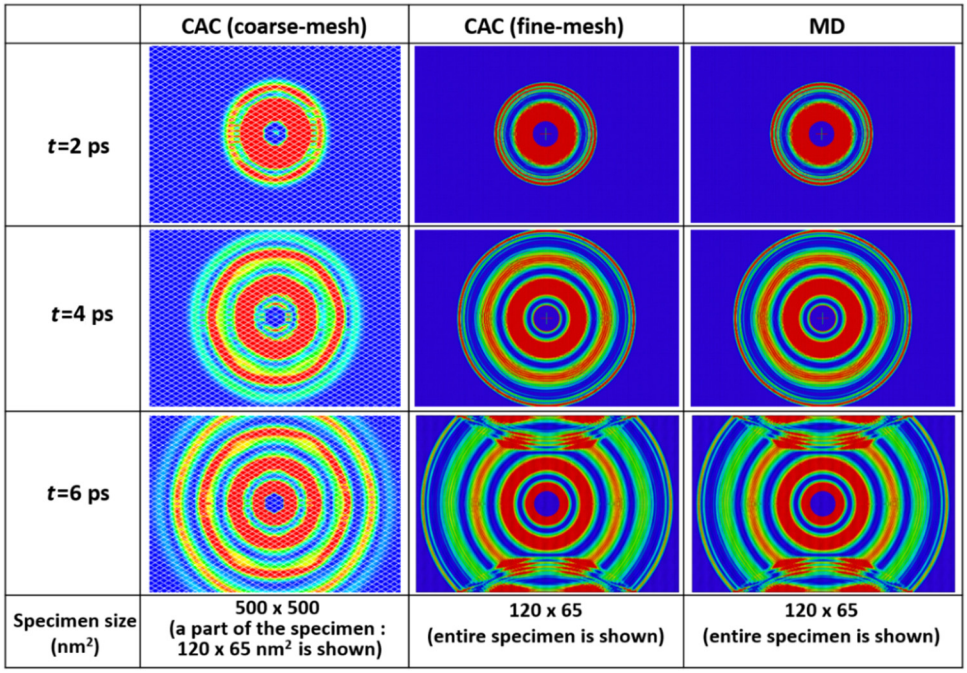


Figure 3. Comparison of a monochromatic wave propagation in CAC with coarse mesh, fines mesh, and in MD.

continuously generate phonons with wavelengths ranging from 5 to 250 nm. The heat source is applied to the center of the models where the coarse elements are employed; the spot size of the heater is 10 nm to avoid strong phonon–phonon scattering.

In Fig. 4, the normalized kinetic energy distributions in the single-crystal models with uniform meshes [Figs. 4(a)–4(c)] and non-uniform meshes [Figs. 4(d)–4(f)] at the same time steps are compared; there is no noticeable difference. The

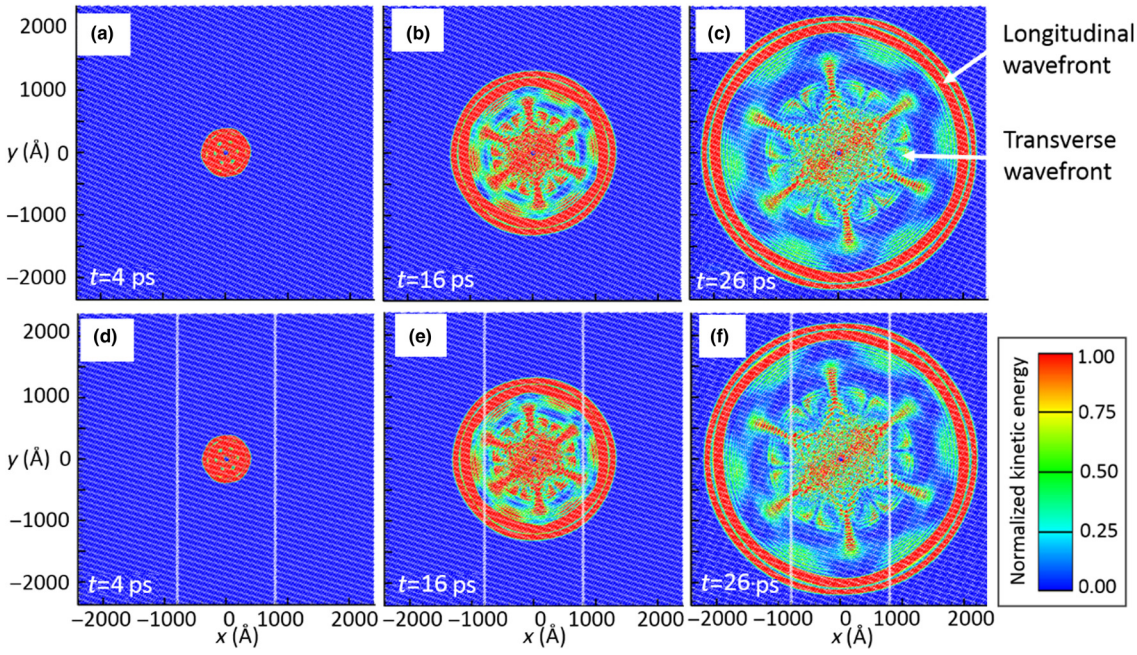


Figure 4. Comparison of the phonon wave propagation in a single-crystal specimen constructed with uniform coarse meshes (a–c) and non-uniform meshes with both atomic and coarse-scale finite element meshes (d–f).

https://doi.org/10.1557/mrc.2017.116 Published online by Cambridge University Press

maximum error is then quantified by comparing the pointwise total kinetic energy in different regions, which is <0.5%. This result confirms that the atomistic–continuum interface in CAC does not provide a numerical barrier for the dynamic propagation of long-wavelength phonons. It is also noticed that relatively short-wavelength phonons channel along the [112] crystal directions and result in phonon-focusing "caustics," which are especially high phonon fluxes along certain directions arising from crystallographic anisotropy. This indicates that CAC method is able to capture experimentally observed phonon-focusing phenomena.[45] In addition, the longitudinal and transverse wavefronts are indicated in Fig. 4(c). The associated wave speeds are measured from the time sequence, as ~6700 and ~3900 m/s, respectively, which are consistent with the phonon group velocities of the LA and TA phonons near the Γ-point from LD calculations. These verifications once again demonstrate the capability of CAC to predict long-wavelength phonon dynamics in crystalline materials.

CAC simulations of coupled phonon transport and defect dynamics

Phonon transport across GBs

Interfaces play a significant role in thermal transport in crystalline materials. However, modeling and simulation of phonon–interface interaction has been historically challenging, especially for incoherent interfaces such as high-angle GBs.[55] Moreover, coupling transport simulation to structural simulation has been identified as a significant challenge in phonon transport.[4] In this section, we demonstrate the capabilities of CAC to simulate the dynamic interaction of a heat pulse with GBs.

Figures 5(a)–5(c) present the time sequences of the normalized kinetic energy obtained from CAC simulations of the propagation of a heat pulse across ∑19 GBs, with the inclination angle between the crystalline grains being 13.2°. More details regarding the computer models and the simulation results have been reported in one of our recent works.[56] Figure 5 clearly demonstrates the coexistence of ballistic and diffusive phonon transport, as well as the coexistence of coherent and incoherent phonon scattering. Figure 5(d) presents the energy transmission across the specimen with and without GBs. This comparison, along with the discontinuities in kinetic energy shown in Fig. 5(c), provides a quantitative understanding of the GB resistance to heat flow. The combination of the diffusive scattering of coherent and incoherent phonons and the reflection of the coherent phonons by the GBs leads to the Kapitza resistance to heat flow in the simulated specimen, as shown in Figs. 5(a)–5(c). Moreover, with a selected input phonon mode, the wavelength-dependent energy transmission has been measured,[56] which shows the capability of CAC to conduct a mode-wise study.

In addition to the qualitative and quantitative study of the effect of GBs on the phonon transport, the spatial and temporal resolved simulation results from CAC can simultaneously capture the defect structural evolution. As shown in Figs. 6(a)–6(d), during the dynamic process, we find that GBs undergo local reconstruction when meeting with phonon caustics of high-energy flux. Depending on the phonon intensity, the reconstruction may occur with or without recovery. The four figures on the top of Figs. 6(a)–6(d) are the exploded views, showing the atomic details of a local GB region during the dynamic interaction with phonons. Note that the white dashed lines mark the initial position of the GB. These simulation results demonstrate that the defect structures can dynamically respond during the phonon transport process. The CAC method along with the CPP model is thus demonstrated to provide a fully coupled treatment of defect dynamics and phonon transport; this is non-trivial for other existing methods that either treat a defect as a static input or consider it through the extrinsic scattering rate of phonons. Figure 6 also points to the significance of long-wavelength phonons on the dynamic evolution of microstructures.

In addition, simulation results show that the majority of the heat is carried by long-wavelength phonons that were not believed to be the major heat carrier. Distinct from the heat propagation in a single crystal, in a polycrystalline material, most of the short-wavelength phonons far away from the Γ-point are confined within the heat-source-grain by the GBs. Therefore, it is the propagation of long-wavelength phonons across the GBs outside the heat-source-grain that determines the capability of a polycrystalline material to conduct heat via phonons. The simulation results demonstrate the capability of

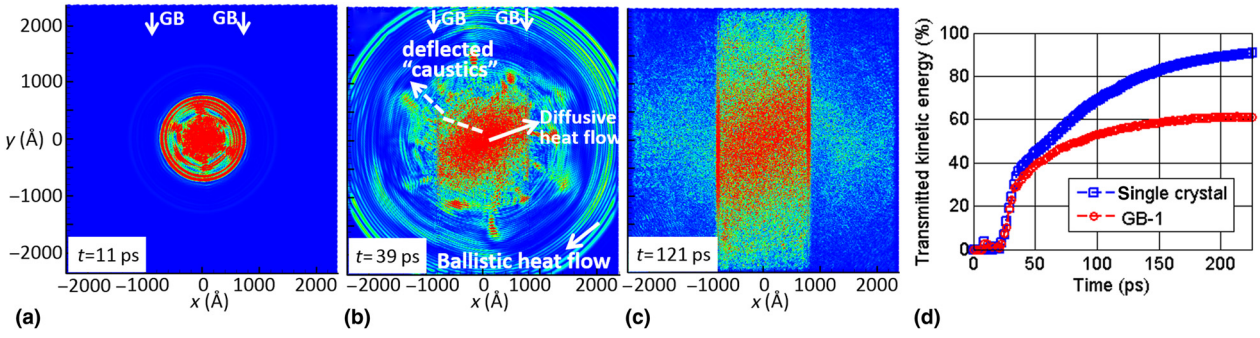


Figure 5. Transient phonon heat propagation in the GB-1 model. The time sequences of the kinetic energy distribution in the GB-1 model are presented in (a–c). The transmitted kinetic energy of the GB-1 mode and that of the single-crystal model during the dynamic process are presented in (d).

https://doi.org/10.1557/mrc.2017.116 Published online by Cambridge University Press

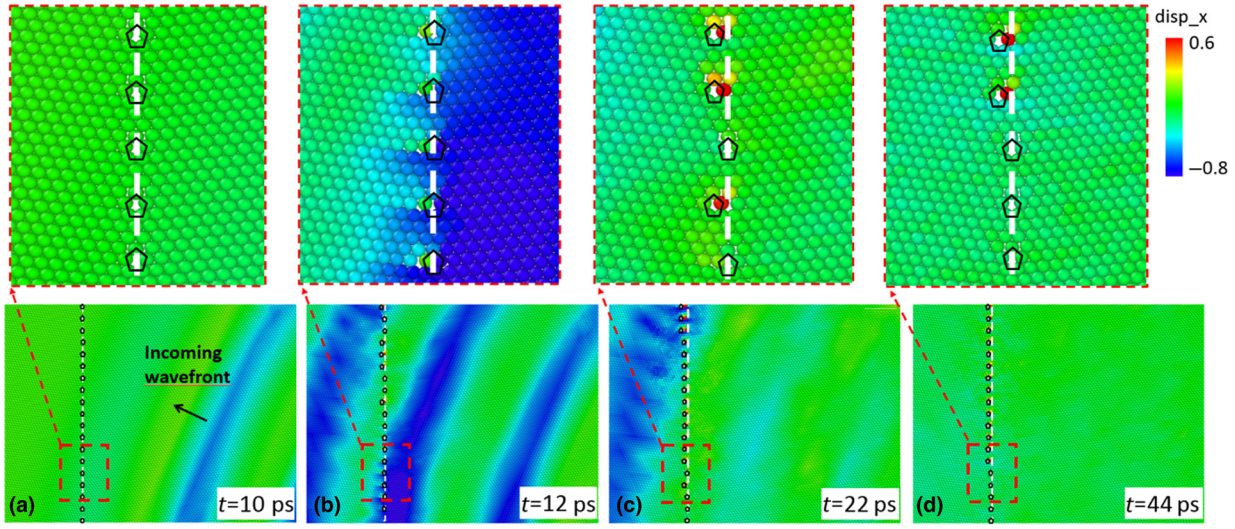


Figure 6. Time sequences of atomic arrangements showing the GB structural change due to the phonon-GB scattering; (a–d) are snapshots taken in the vicinity of the GB region where the GB intersects with the energy caustics of the phonon pulse. Corresponding to each figure, there is an exploded view of the highlighted region (in red dash line). The white dashed line marks the initial position of the GB.

CAC in the simulation of heat pulse propagation in polycrystalline materials via phonon transport.

Wave interference in superlattices

Wave interference is believed to play a significant role in phonon transport in periodic superlattices. However, detecting this transient process requires extremely fine temporal and spatial resolutions; a direct experimental observation is thus prohibited. Instead, indirect supporting evidence, such as the existence of the minimum thermal conductivity as a function of the superlattice period length[57–62] and the linear size dependence of the superlattice thermal conductivity,[52] are considered to be indicative of the phonon wave interference effect.

In this section, we demonstrate the capability of CAC to provide direct visualization of the wave interference phenomena in superlattices. Computer models of superlattices are constructed with two types of materials (A and B) governed by LJ interatomic potential. The ratios of the atomic masses, the zero-crossing distances and the dielectric constants of the two materials are, respectively, $m_A/m_B = 1.2$, $\sigma_A/\sigma_B = 1.0$ and $\varepsilon_A/\varepsilon_B = 5.0$. Three superlattices of equal size but different period lengths are modeled and simulated. With the propagation of a monochromatic phonon wave (106.3 nm in wavelength), the kinetic energy distribution in the three models presented in Figs. 7(a)–7(c) shows distinct responses. In Fig. 7(a), the phase interfaces in the superlattice structure behave independently and the wavelength changes alternatively in different material layers. In Fig. 7(b), we observe that the phonon wave propagating in the direction perpendicular to interfaces is completely reflected back by the interfaces; this provides a direct visual evidence of Bragg reflection.[19] Figure 7(c) shows that the superlattice behaves in this case like a homogeneous material, with the phonon wave traveling across it ballistically. These simulation results demonstrate

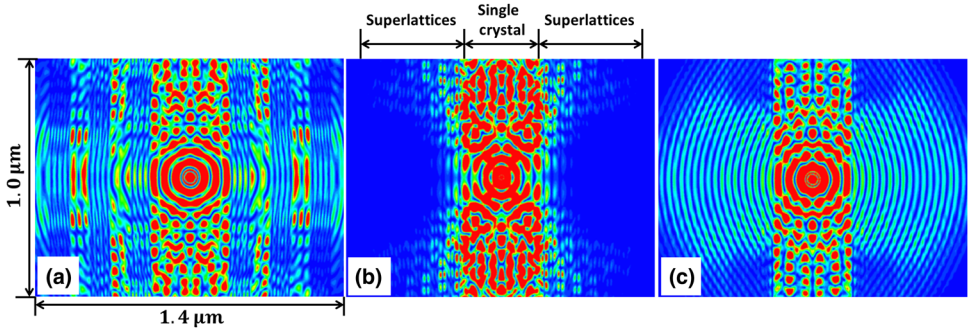


Figure 7. Snapshots of normalized kinetic energy distribution during the propagation of a same monochromatic phonon wave (with a wavelength of 106.3 nm) in three superlattices of equal size but different period lengths (a) 177.1 nm, (b) 35.4 nm, and (c) 17.7 nm.

https://doi.org/10.1557/mrc.2017.116 Published online by Cambridge University Press

that, without an assumption regarding the nature of phonon transport, i.e., whether it is particle-like or wave-like, the wave-like transport phenomenon naturally emerges in the CAC simulation of superlattices.

Phonons scattering by moving dislocations

Simulation of fast-moving dislocations is non-trivial. Most of the existing studies have considered dislocations under static or quasi-static conditions.[60,63–68] For the study of multiple dislocations, the dislocation spacing is usually assumed to be sufficiently large, so that the interactions are decoupled.[69] To provide an understanding of the fast-moving dislocation at the atomic level, MD has demonstrated its predictive capability. However, the long-range nature associated with the phenomenon of moving dislocations, especially multiple moving dislocations, as well as their interaction with propagating phonons, is beyond the length scale of MD at reasonably affordable computational cost. The CAC method can be used to complement MD to provide this information. A verification study of the CAC method in modeling fast-moving dislocations has been reported.[70] One of our recent works has presented a phonon pulse propagation in crystalline materials with a fast-moving dislocation and dislocation array while studying the effect of phonons on dislocation mobility.[71]

Figure 8 presents the kinetic energy distributions at the vicinity of the dislocation cores during the process of nucleation and migration of a single dislocation [Figs. 8(a)–8(d)] and an array of multiple dislocations [Figs. 8(e)–8(h)]. The time sequences show that the dislocation motion is accompanied by a V-shape pattern of strong lattice vibrations in the wake of the moving dislocation, together with the relatively weak radial-shape wave front; this is consistent with a recent MD study on a single dislocation.[72] The dynamic process presented in Fig. 8 also shows that the radial wave front propagates faster than the dislocation core, indicating subsonic dislocation motion. This also explains why the wave interference band in Figs. 8(f)–8(h) widens as the dislocation array advances. In addition, our simulation results show that a dislocation can travel to microns before its velocity reaches a steady-state condition[71]; this explains the size effect in MD.[73,74]

Figure 9 presents the interaction between a moving dislocation array and a propagating phonon pulse. The domain size is 5 μm by 5 μm. It is shown that during the process, multiple phonon scattering mechanisms coexist and cannot be simply decoupled. Therefore, it is important to naturally incorporate

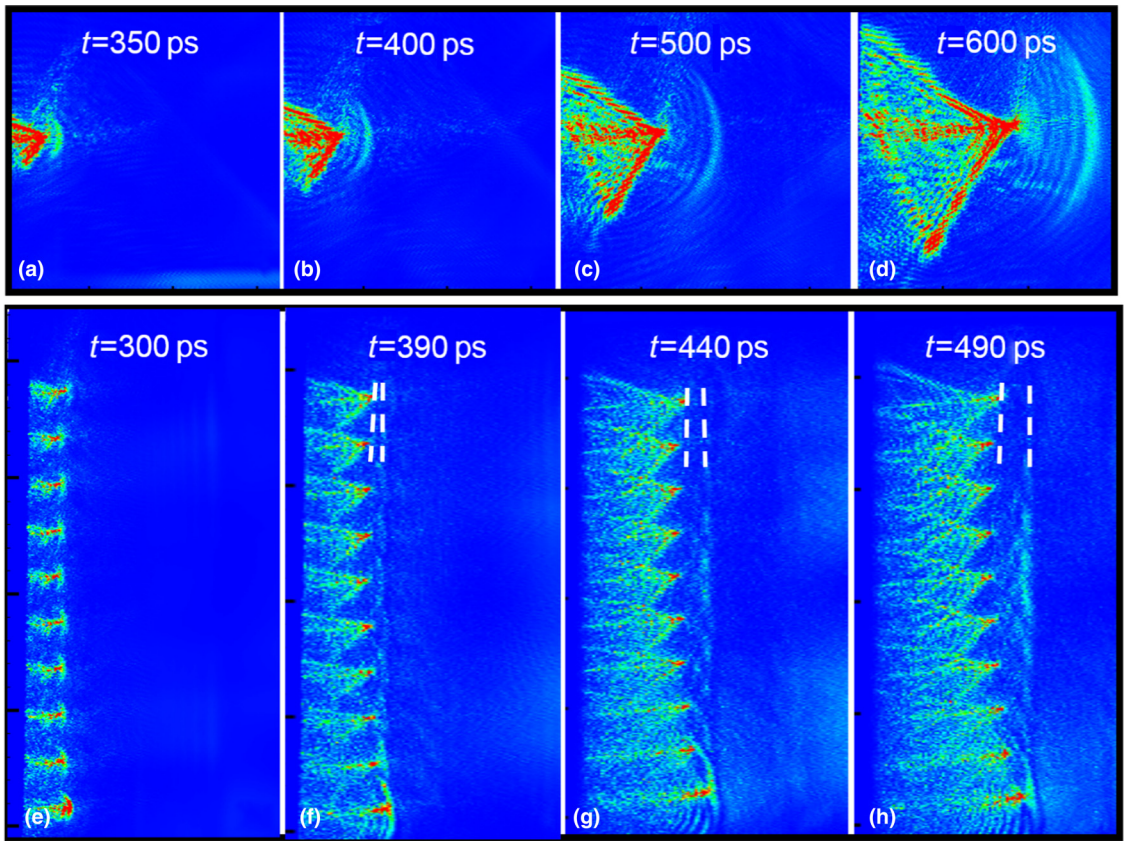


Figure 8. Time sequences of the kinetic energy distributions at the vicinity of the dislocation cores during the process of nucleation and migration of a single (a–d) and multiple dislocations (e–h), and phonon waves emitted from dislocations.

https://doi.org/10.1557/mrc.2017.116 Published online by Cambridge University Press

all the scattering events without additional assumptions regarding either the individual scattering mechanism or a rule that combines them. For example, with multiple dislocations, the strong wave interference band scatters the incoming phonon pulse before the phonons meet with the dislocations, as shown in Fig. 9(a). This in turn, changes the mobility of the dislocation when it is in the array compared to when it is present alone.[71] Fig. 9(b) shows that during the interaction, one of the dislocations starts to decelerate by emitting phonon waves from the dislocation core and is soon arrested. After the wave front passes by, as shown in Fig. 9(c), three dislocations (with red dislocation marks) out of ten are arrested. The simulation of fast-moving dislocations interacting with the phonon pulse once again demonstrates that CAC is able to provide a fully coupled treatment of defect dynamics and phonon transport. In addition, the spatial and temporal resolved simulation results have allowed a detailed investigation of the dynamic processes and their underlying physics.

Heat-flux formula for transient transport processes and inhomogeneous materials

Momentum and heat fluxes in the majority of literature and in popular MD simulators are defined as "a quantity per unit volume." The most popular expressions of such volume-averaged fluxes include the virial theorem for stress, the heat theorem for energy flux,[75,76] and many atomistic formulations that followed the Irving–Kirkwood's statistical mechanical formalism[21] such as the Hardy formulas.[77] However, defining a flux as a quantity per volume is a fundamental departure from the physical definition of a flux as "a physical property across a surface per unit area and time."[21] Consequently, these volume-averaged flux formulas have been shown to be inapplicable to transient transport processes or highly inhomogeneous system.[10,78]

CAC is fundamentally a space- and time-resolved simulation tool. It aims for simulations of non-equilibrium transient processes in mesoscale hierarchical materials. This requires that the methodology for measuring fluxes be free of constitutive relations, except for the interatomic potential, and that space- and time-resolved fluxes in the transient non-equilibrium simulations can be accurately measured. For this purpose, a new method is recently formulated for formally deriving microscopic momentum and heat fluxes through the integral conservation laws.[10] The resulting flux formulas are defined as surface averages, i.e.,

$$\boldsymbol{\sigma}(\boldsymbol{x},t) = -\sum_k m_k \tilde{v}_k^\alpha \tilde{v}_k^\beta \boldsymbol{e}^\alpha \bar{\delta}_{AT}^\beta(\boldsymbol{r}_k - \boldsymbol{x}) - \sum_{k,l} \frac{\partial \Phi_l}{\partial r_k^\alpha} \int_{\boldsymbol{L}_{kl}} \bar{\delta}_{AT}^\beta(\boldsymbol{\varphi} - \boldsymbol{x}) d\boldsymbol{\varphi} \boldsymbol{e}^\alpha \boldsymbol{e}^\beta, \quad (2)$$

$$\boldsymbol{q}(\boldsymbol{x},t) = -\sum_k \tilde{v}_k^\alpha [\tfrac{1}{2} m^k (\tilde{\boldsymbol{v}}_k)^2 + \Phi_k] \bar{\delta}_{AT}^\alpha(\boldsymbol{r}_k - \boldsymbol{x}) + \sum_{k,l(\neq k)} \frac{\partial \Phi_l}{\partial \boldsymbol{r}_k} \cdot \tilde{\boldsymbol{v}}_k \int_{\boldsymbol{L}_{kl}} \bar{\delta}_{AT}^\alpha(\boldsymbol{\varphi} - \boldsymbol{x}) d\boldsymbol{\varphi} \boldsymbol{e}^\alpha, \quad (3)$$

where m_k, $\boldsymbol{r}_k$, $\boldsymbol{v}_k$, Φ_k are the mass, position, velocity, potential energy of the kth particle, respectively; $\boldsymbol{e}^{\boldsymbol{\alpha}}$ or $\boldsymbol{e}^{\boldsymbol{\beta}}$ denotes the unit basis, and α and β are summation indices; $\bar{\delta}_{AT}^\alpha(\boldsymbol{r}_k - \boldsymbol{x})$ is the averaged Dirac Delta over time interval T and surface element A^α whose normal is $\boldsymbol{e}^{\boldsymbol{\alpha}}$. The quantity $\int_{\boldsymbol{L}_{kl}} \bar{\delta}_A^\alpha(\boldsymbol{\varphi} - \boldsymbol{x}) d\boldsymbol{\varphi}$ is the line integral of the averaged Dirac Delta over the line segment $\boldsymbol{L}_{kl}$ that links particle k and l; it is typically equal to one or zero based on whether the pair of particles intersects the surface.

These new surface-averaged flux formulas have been shown to reproduce uniquely known values of the stress and heat flux in the equilibrium state, the steady-state, and the transient transport processes. Here we provide simulations of two inhomogeneous systems to demonstrate the applicability of the surface-averaged

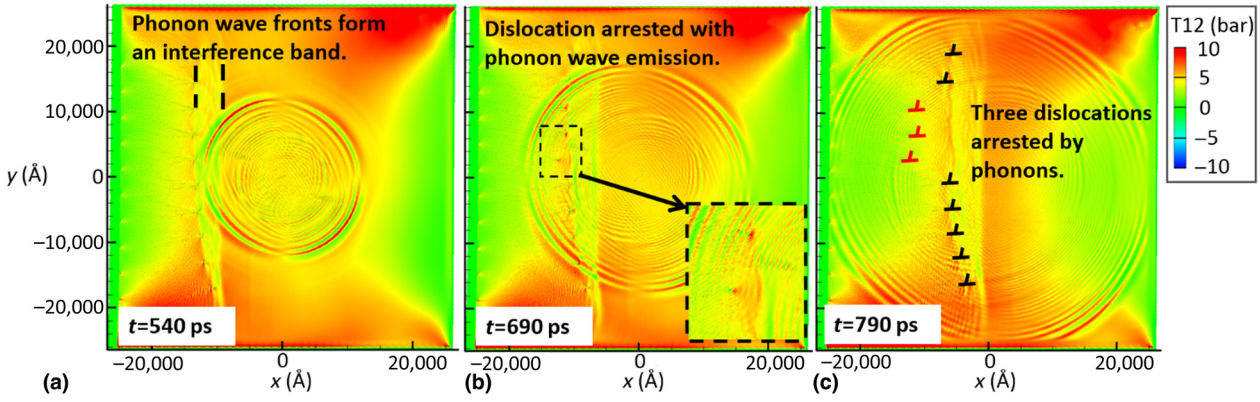


Figure 9. Time sequences of the shear stress distributions show the propagating heat pulse interactions with multiple moving dislocations. (a) Multiple dislocations moving in an array and a phonon pulse propagates toward the moving dislocations. (b) After interaction with the phonon pulse, one of the dislocations starts to decelerate through wave emission. (c) Three out of ten moving dislocations are arrested after interaction with the phonon pulse.

https://doi.org/10.1557/mrc.2017.116 Published online by Cambridge University Press

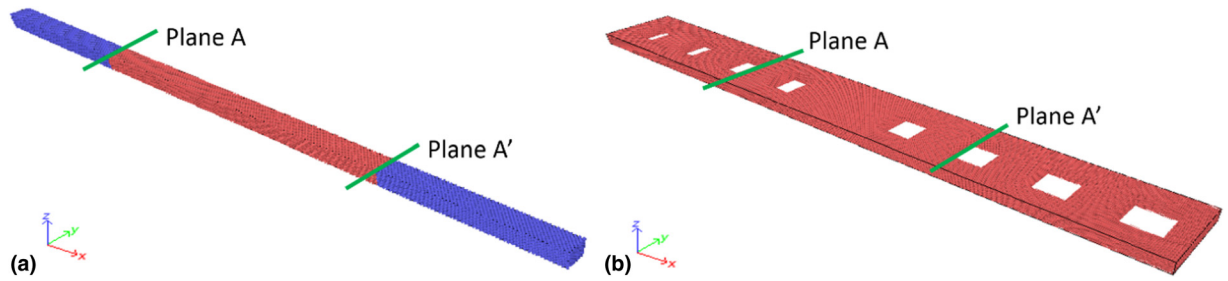


Figure 10. Computer model of (a) a superlattice structure with length 100 nm and a cross-section of 3 × 3 nm; (b) a symmetric Si structure of dimension 2400 × 270 × 50 Å with holes. The interfaces at which planes intersect the model cross-section to measure flux are denoted by the green lines.

formula for energy flux in transient transport processes: a LJ superlattice structure in Fig. 10(a) and a Stillinger–Weber Si phononic crystal in Fig. 10(b).

The results of energy flux from different formulas are plotted in Figs. 11 and 12. The results using the surface-averaged energy flux formula, labeled as "*surface*," are compared with the energy flux that satisfies the continuity equation, labeled as "*continuum*," and the volume-averaged heat-flux formula, labeled as "*volume*." Here, the "*continuum*" energy flux formula is based on the hydrodynamics continuity equation through measuring the change of the total energy in a region to obtain the flow of energy across the entire surface enclosing the region[79]; it is also the formula widely used in non-equilibrium MD simulations with the heat-source-sink scheme to calculate the heat flux in steady-state heat flow. Meanwhile, the "*volume*" formula is widely used in equilibrium MD simulations using the Green–Kubo formalism to compute thermal conductivity. Since the Hardy fluxes are volume averages that produce similar results to the virial and heat theorems,[80,81] we only plot the energy flux based on the heat theorem as the medium of comparison for volume averages. It is noted that the "*continuum*" formula measures the total energy flux across the entire surface rather than the local energy flux. However, with periodic boundary conditions being applied in both the ***y***- and ***z***-directions, the total energy flux averaged over two symmetrically located planes A and A′ is equal to the averaged local energy flux over the area of the two planes.

Both the simulation results of the superlattice and the phononic crystal show that the transient energy flux across the interfaces predicted by the "*surface*" formula compares well with that of the "*continuum*" formula during the propagation of the heat pulses. By contrast, the "*volume*" formula significantly underestimates the transient energy flux in the superlattice, as shown in Fig. 11, and exhibits spurious fluctuations in the phononic crystal model, as shown in Fig. 12, when attempting a transient local computation of heat flux. These simulations demonstrate that the surface formula is in accordance with the total energy rate of change experienced by the chosen volume, and is capable of measuring energy flux in space- and time-resolved atomistic or coarse-grained atomistic simulations.

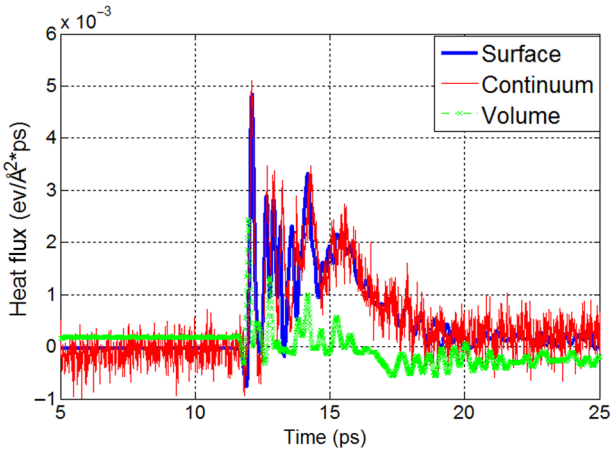


Figure 11. Energy flux during the transient simulation of the propagation of a heat pulse in the superlattice, averaged over two symmetric planes A and A′. Each data point is averaged over 100 time steps. The pulse inputs a total of 100 eV over 10 fs to the center region of the model.

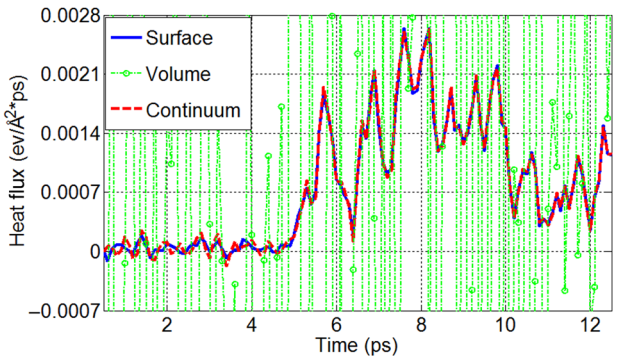


Figure 12. Energy flux during the transient simulation of the propagation of a heat pulse in the holey silicon structure, averaged over two symmetric planes A and A′. Each data point is averaged over 100 time steps. The pulse inputs a total of 100 eV over 10 fs to the center region of the model.

https://doi.org/10.1557/mrc.2017.116 Published online by Cambridge University Press

Summary and discussions

In summary, we have introduced the recent progress in the development and application of the CAC method. First, the predictive capabilities of CAC in the realm of phonon dynamics are verified through (1) comparison of phonon dispersion relations obtained by CAC with that by LD; (2) agreement of wave propagation in CAC with that in MD; and (3) phonon transport across the numerical interfaces between fully resolved atomistic and coarse-grained continuum domain. The CAC method is shown to be able to accurately reproduce the dynamics of an atomistic system if modeled with the finest mesh and, if discretized with coarse-scale finite elements, it can predict the dynamics of phonons with wavelengths longer than a critical wavelength determined by the size of the element. The atomistic–continuum interface does not act as a numerical barrier or induce spurious wave reflection for long-wavelength phonons. Three numerical examples are then presented to demonstrate the capability of CAC to address one of the major challenges in the field – to concurrently couple phonon transport and structural dynamics in a simulation with one single set of governing laws, with full coupling of transport and mesoscale defect structures and their evolution resolved in a simulation domain of sufficient size at the mesoscale. Specifically,

(1) Since CAC is derived bottom–up from atomistics in phase space, the structure of defects can naturally be resolved both spatially and temporally. The theoretical foundation of CAC facilitates the introduction of the new phonon representation of heat pulses, and results in the coupling of defect dynamics to phonon transport. This recent development of CAC is a step forward in addressing the major challenge in the field, which aims to extend the length scale of ordinary MD simulations to study mesoscopic transport phenomena in materials. CAC is able to capture the dynamic reconstructive character of microstructures in response to phonon scattering at higher length scales, which is critically important for the study of multiple boundaries associated with hierarchical structures, defects with irregular structures such as incoherent GBs, dynamic evolution of defects that manifest long-range interactions, e.g., multiple moving dislocations.
(2) The simulation results provide visual evidence for a variety of phenomena without any a priori understanding or assumptions regarding phonon transport or phonon-defect scattering. All the dynamic processes involved in the CAC simulation are determined only by Newton's law of motion, the interatomic potential, and the material microstructure. If multiple defects are modeled in one simulation domain, all scattering events are naturally included; coupled scattering mechanisms can thus be predicted without any assumption such as the Mathiessen's rule employed in the BTE method.
(3) The recent development in CAC shows the capability of the method to mimic the dynamic, in situ experimental studies of non-equilibrium transient transport processes in material samples that are at length scales typically inaccessible by MD. This is a step forward in filling the gap between computational simulation and field experiments at the mesoscale.

Quantum-mechanical computational packages based on the DFT allow a predictive, parameter-free study of the role of atomic bonding and phonon–phonon scattering,[82] which can be used to predict the thermal conductivity of simple crystals. Although the extension to complex crystals with a rigorous treatment of disorder and boundaries requires further advances, accurate interatomic potentials DFT may provide can further enhance the predictive power of the atomistic simulations, as well as the coarse-grained atomistic simulations such as CAC. For defects with small characteristic length, simulation tools such as MD can simultaneously capture the full atomistic picture of both the phonon thermal transport and structural evolution. To capture that picture for defects and structures with larger characteristic length, or materials with multiple defects, a coarse-graining technique such as that used in CAC holds the promise to provide useful insights.

Recent advances in experimental and computational techniques have enabled an unprecedented microscopic view of materials mechanical and thermal transport. However, many aspects of the fundamental microscopic details, as well as the connection between experimental observations and the simulation results, are still lacking.[3,83] Collaboration among these communities is needed to integrate information from investigations performed at different scales and/or from different perspectives. CAC aims to meet the need in the field for a simulation tool that fully couples material microstructure, mechanical, and thermal transport behavior via phonons. It is capable of including both coherent and incoherent scattering processes in materials with microstructure, as well as defect dynamics and phonon transport.

Acknowledgments

This material is based upon research supported by the US Department of Energy, Office of Science, Basic Energy Sciences, Division of Materials Sciences and Engineering under Award #DE-SC0006539.

References

1. U.S.D.o.E. Office of Science: Computational Materials Science and Chemistry – Accelerating Discovery and Innovation through Simulation-Based Engineering and Science (2010).
2. S.V.J. Narumanchi, J.Y. Murthy, and C.H. Amon: Boltzmann transport equation-based thermal modeling approaches for hotspots in microelectronics. *Heat Mass Transf.* **42**, 478 (2006).
3. A.J. Minnich: Advances in the measurement and computation of thermal phonon transport properties. *J. Phys. Condens. Matter* **27**, 053202 (2015).
4. G. Chen: Multiscale simulation of phonon and electron thermal transport. *Annu. Rev. Heat Transf.* **17**, 1 (2014).
5. N. Mingo and L. Yang: Phonon transport in nanowires coated with an amorphous material: an atomistic Green's function approach. *Phys. Rev. B* **68**, 245406 (2003).

https://doi.org/10.1557/mrc.2017.116 Published online by Cambridge University Press

6. S. Sadasivam, Y. Che, Z. Huang, L. Chen, S. Kumar, and T.S. Fisher: The atomistic Green's function method for interfacial phonon transport. *Annu. Rev. Heat Transf.* **17**, 89 (2014).
7. D.G. Cahill, W.K. Ford, K.E. Goodson, G.D. Mahan, A. Majumdar, H. J. Maris, R. Merlin, and S.R. Phillpot: Nanoscale thermal transport. *J. Appl. Phys.* **93**, 793 (2003).
8. A. Chernatynskiy, D. R. Clarke, and S. R. Phillpot: Thermal transport in nanostructured materials, in *Handbook of Nanoscience, Engineering, and Technology*, 3rd ed., edited by W.A. Goddard III, D.W. Brenner, S. E. Lyshevski and G.J. Iafrate (CRC Press, Boca Raton, 2012), p. 545.
9. Y. Chalopin, A. Rajabpour, H. Han, Y. Ni, and S. Volz: Modeling heat conduction from first principles. *Annu. Rev. Heat Transf.* **17**, 147 (2014).
10. Y. Chen and A. Diaz: Local momentum and heat fluxes in transient transport processes and inhomogeneous systems. *Phys. Rev. E: Stat. Phys. Plasmas Fluids* **94**, 053309 (2016).
11. P. Jund and R. Jullien: Molecular-dynamics calculation of the thermal conductivity of vitreous silica. *Phys. Rev. B* **59**, 13707 (1999).
12. A. Bagri, S.-P. Kim, R.S. Ruoff, and V.B. Shenoy: Thermal transport across twin grain boundaries in polycrystalline graphene from nonequilibrium molecular dynamics simulations. *Nano Lett.* **11**, 3917 (2011).
13. M. Hu and D. Poulikakos: Si/Ge superlattice nanowires with ultralow thermal conductivity. *Nano Lett.* **12**, 5487 (2012).
14. Y.K. Koh, Y. Cao, D.G. Cahill, and D. Jena: Heat-transport mechanisms in superlattices. *Adv. Funct. Mater.* **19**, 610 (2009).
15. K.T. Regner, D.P. Sellan, Z. Su, C.H. Amon, A.J.H. McGaughey, and J. A. Malen: Broadband phonon mean free path contributions to thermal conductivity measured using frequency domain thermoreflectance. *Nat. Commun.* **4**, 1640 (2013).
16. Y. Chen, J. Zimmerman, A. Krivtsov, and D.L. McDowell: Assessment of atomistic coarse-graining methods. *Int. J. Eng. Sci.* **49**, 1337 (2011).
17. M.T. Dove: *Introduction to Lattice Dynamics* (Cambridge University Press, Cambridge; New York, 1993).
18. B.E.S.A. Committee: From Quanta to the Continuum: Opportunities for Mesoscale Science, edited by U. S. D. o. Energy (2012).
19. C. Kittel: *Introduction to Solid State Physics* (Wiley, New York, 1966).
20. J.H. Irving and J.G. Kirkwood: The statistical mechanical theory of transport processes. IV. The equations of hydrodynamics. *J. Chem. Phys.* **18**, 817 (1950).
21. J.G. Kirkwood: The statistical mechanical theory of transport processes I. General theory. *J. Chem. Phys.* **14**, 180 (1946).
22. A.C. Eringen: *Mechanics of Micromorphic Continua* (Defense Technical Information Center, Ft. Belvoir, 1967).
23. A.C. Eringen: *Microcontinuum Field Theories: I. Foundations and Solids* (Springer, New York, 2012).
24. Y. Chen and J.D. Lee: Connecting molecular dynamics to micromorphic theory. (I). Instantaneous and averaged mechanical variables. *Phys. A: Stat. Mech. Appl.* **322**, 359 (2003).
25. Y. Chen and J.D. Lee: Connecting molecular dynamics to micromorphic theory. (II). Balance laws. *Phys. A: Stat. Mech. Appl.* **322**, 377 (2003).
26. Y. Chen, J.D. Lee, and A. Eskandarian: Atomistic counterpart of micromorphic theory. *Acta Mech.* **161**, 81 (2003).
27. Y. Chen and J.D. Lee: Determining material constants in micromorphic theory through phonon dispersion relations. *Int. J. Eng. Sci.* **41**, 871 (2003).
28. Y. Chen: Reformulation of microscopic balance equations for multiscale materials modeling. *J. Chem. Phys.* **130**, 134706 (2009).
29. Y. Chen and J. Lee: Atomistic formulation of a multiscale theory for nano/micro physics. *Philos. Mag. A* **85**, 4095 (2005).
30. Y. Chen: Local stress and heat flux in atomistic systems involving three-body forces. *J. Chem. Phys.* **124**, 054113 (2006).
31. Y. Chen, J.D. Lee, and A. Eskandarian: Atomistic viewpoint of the applicability of microcontinuum theories. *Int. J. Solids Struct.* **41**, 2085 (2004).
32. Y. Chen, J.D. Lee, and A. Eskandarian: Examining the physical foundation of continuum theories from the viewpoint of phonon dispersion relation. *Int. J. Eng. Sci.* **41**, 61 (2003).
33. Q. Deng, L. Xiong, and Y. Chen: Coarse-graining atomistic dynamics of brittle fracture by finite element method. *Int. J. Plast.* **26**, 1402 (2010).
34. Q. Deng and Y. Chen: A coarse-grained atomistic method for 3D dynamic fracture simulation. *Int. J. Multiscale Comput. Eng.* **11**, 227 (2013).
35. Q. Deng: *Coarse-graining Atomistic Dynamics of Fracture by Finite Element Method: Formulation, Parallelization and Applications* (University of Florida, Gainesville, Florida, 2011), p. 124.
36. L. Xiong and Y. Chen: Coarse-grained simulations of single-crystal silicon. *Model. Simul. Mater. Sci. Eng.* **17**, 035002 (2009).
37. L. Xiong, S. Xu, D.L. McDowell, and Y. Chen: Concurrent atomistic–continuum simulations of dislocation–void interactions in fcc crystals. *Int. J. Plast.* **65**, 33 (2015).
38. S. Yang, L. Xiong, Q. Deng, and Y. Chen: Concurrent atomistic and continuum simulation of strontium titanate. *Acta Mater.* **61**, 89 (2013).
39. L. Xiong, D.L. McDowell, and Y. Chen: Nucleation and growth of dislocation loops in Cu, Al and Si by a concurrent atomistic-continuum method. *Scr. Mater.* **67**, 633 (2012).
40. L. Xiong, G. Tucker, D.L. McDowell, and Y. Chen: Coarse-grained atomistic simulation of dislocations. *J. Mech. Phys. Solids* **59**, 160 (2011).
41. L. Xiong, Q. Deng, G.J. Tucker, D.L. McDowell, and Y. Chen: Coarse-grained atomistic simulations of dislocations in Al, Ni and Cu crystals. *Int. J. Plast.* **38**, 86 (2012).
42. L. Xiong, Q. Deng, G. Tucker, D.L. McDowell, and Y. Chen: A concurrent scheme for passing dislocations from atomistic to continuum domains. *Acta Mater.* **60**, 899 (2012).
43. L. Xiong and Y. Chen: Coarse-grained atomistic modeling and simulation of inelastic material behavior. *Acta Mech. Solida Sinica* **25**, 244 (2012).
44. S. Yang, N. Zhang, and Y. Chen: Concurrent atomistic–continuum simulation of polycrystalline strontium titanate. *Philos. Mag.* **95**, 2697 (2015).
45. J.P. Wolfe: *Imaging Phonons: Acoustic Wave Propagation in Solids* (Cambridge University Press, Cambridge, U.K.; New York, 1998).
46. A.J. Schmidt: *Optical Characterization of Thermal Transport from the Nanoscale to the Macroscale, in Mechanical Engineering* (Massachusetts Institute of Technology, Cambridge, Massachusetts, 2008).
47. R.J. Stoner and H.J. Maris: Picosecond optical study of the Kapitza Conductance between metals and dielectrics at high temperature, in *Phonon Scattering in Condensed Matter VII*, edited by M. Meissner and R. Pohl (Springer, Berlin Heidelberg, 1993), p. 401.
48. P.E. Hopkins, R.J. Stevens, and P.M. Norris: Influence of inelastic scattering at metal-dielectric interfaces. *J. Heat Transf.* **130**, 022401 (2008).
49. A.N. Smith, J.L. Hostetler, and P.M. Norris: Thermal boundary resistance measurements using a transient thermoreflectance technique. *Microscale Thermophys. Eng.* **4**, 51 (2000).
50. D.H. Hurley, S.L. Shinde, and V.E. Gusev: Lateral-looking time-resolved thermal wave microscopy. *J. Korean Phys. Soc.* **57**, 384 (2010).
51. D. Hurley, S.L. Shindé, and E.S. Piekos: Interaction of thermal phonons with interfaces, in *Length-Scale Dependent Phonon Interactions*, edited by L.S. Shindé and P.G. Srivastava (Springer, New York, 2014), p. 175.
52. M.N. Luckyanova, J. Garg, K. Esfarjani, A. Jandl, M.T. Bulsara, A. J. Schmidt, A.J. Minnich, S. Chen, M.S. Dresselhaus, Z. Ren, E. A. Fitzgerald, and G. Chen: Coherent phonon heat conduction in superlattices. *Science* **338**, 936 (2012).
53. X. Chen, A. Chernatynskiy, L. Xiong, and Y. Chen: A coherent phonon pulse model for transient phonon thermal transport. *Comput. Phys. Commun.* **195**, 112 (2015).
54. Y. Kogure, T. Tsuchiya, and Y. Hiki: Simulation of dislocation configuration in rare gas crystals. *J. Phys. Soc. Jpn.* **56**, 989 (1987).
55. G. Chen: Ballistic-diffusive equations for transient heat conduction from nano to macroscales. *J. Heat Transf.* **124**, 320 (2001).
56. X. Chen, W. Li, L. Xiong, Y. Li, S. Yang, Z. Zheng, D.L. McDowell, and Y. Chen: Ballistic-diffusive phonon heat transport across grain boundaries. *Acta Mater.* **136**, 355 (2017).
57. J. Ravichandran, A.K. Yadav, R. Cheaito, P.B. Rossen, A. Soukiassian, S. J. Suresha, J.C. Duda, B.M. Foley, C.-H. Lee, Y. Zhu, A.W. Lichtenberger, J.E. Moore, D.A. Muller, D.G. Schlom, P.E. Hopkins, A. Majumdar, R. Ramesh, and M.A. Zurbuchen: Crossover from incoherent to coherent phonon scattering in epitaxial oxide superlattices. *Nat. Mater.* **13**, 168 (2014).
58. A. Chernatynskiy, R.W. Grimes, M.A. Zurbuchen, D.R. Clarke, and S. R. Phillpot: Crossover in thermal transport properties of natural, perovskite-structured superlattices. *Appl. Phys. Lett.* **95**, 161906 (2009).
59. J. Garg and G. Chen: Minimum thermal conductivity in superlattices: a first-principles formalism. *Phys. Rev. B* **87**, 140302 (2013).

https://doi.org/10.1557/mrc.2017.116 Published online by Cambridge University Press

60. D. Churochkin, F. Barra, F. Lund, A. Maurel, and V. Pagneux: Multiple scattering of elastic waves by pinned dislocation segments in a continuum. *Wave Motion* **60**, 220 (2016).
61. M.V. Simkin and G.D. Mahan: Minimum thermal conductivity of superlattices. *Phys. Rev. Lett.* **84**, 927 (2000).
62. J.R. Lukes and H. Zhong: Thermal conductivity of individual single-wall carbon nanotubes. *J. Heat Transf.* **129**, 705 (2006).
63. J.D. Eshelby: Dislocations as a cause of mechanical damping in metals. *Proc. R. Soc. London, Ser. A* **197**, 396 (1949).
64. F.R.N. Nabarro: The interaction of screw dislocations and sound waves. *Proc. R. Soc. London, Ser. A* **209**, 278 (1951).
65. P.G. Klemens: The scattering of low-frequency lattice waves by static imperfections. *Proc. Phys. Soc.* **68**, 1113 (1955).
66. A. Granato and K. Lücke: Theory of mechanical damping due to dislocations. *J. Appl. Phys.* **27**, 583 (1956).
67. M. Peach and J.S. Koehler: The forces exerted on dislocations and the stress fields produced by them. *Phys. Rev.* **80**, 436 (1950).
68. A. Maurel, V. Pagneux, F. Barra, and F. Lund: Wave propagation through a random array of pinned dislocations: velocity change and attenuation in a generalized Granato and Lucke theory. *Phys. Rev. B* **72**, 174111 (2005).
69. A. Maurel, J.-F. Mercier, and F. Lund: Elastic wave propagation through a random array of dislocations. *Phys. Rev. B* **70**, 024303 (2004).
70. L. Xiong, J. Rigelesaiyin, X. Chen, S. Xu, D.L. McDowell, and Y. Chen: Coarse-grained elastodynamics of fast moving dislocations. *Acta Mater.* **104**, 143 (2016).
71. X. Chen, L. Xiong, D.L. McDowell, and Y. Chen: Effects of phonons on mobility of dislocations and dislocation arrays. *Scr. Mater.* **137**, 22 (2017).
72. H. Koizumi, H.O.K. Kirchner, and T. Suzuki: Lattice wave emission from a moving dislocation. *Phys. Rev. B* **65**, 214104 (2002).
73. S.G. Volz and G. Chen: Molecular-dynamics simulation of thermal conductivity of silicon crystals. *Phys. Rev. B* **61**, 2651 (2000).
74. X.W. Zhou, R.E. Jones, and S. Aubry: Molecular dynamics prediction of thermal conductivity of GaN films and wires at realistic length scales. *Phys. Rev. B* **81**, 155321 (2010).
75. W.G. Hoover: *Computational Statistical Mechanics* (Elsevier Science, Burlington, 2012).
76. W.G. Hoover: *Molecular Dynamics* (Springer Berlin, Berlin, 2013).
77. R.J. Hardy: Formulas for determining local properties in molecular dynamics simulations: shock waves. *J. Chem. Phys.* **76**, 622 (1982).
78. C. Youping: The origin of the distinction between microscopic formulas for stress and Cauchy stress. *Europhys. Lett.* **116**, 34003 (2016).
79. B.D. Todd, P.J. Daivis, and D.J. Evans: Heat flux vector in highly inhomogeneous nonequilibrium fluids. *Phys. Rev. E* **51**, 4362 (1995).
80. J.A. Zimmerman, E.B. WebbIII, J.J. Hoyt, R.E. Jones, P.A. Klein, and D. J. Bammann: Calculation of stress in atomistic simulation. *Model. Simul. Mater. Sci. Eng.* **12**, S319 (2004).
81. I. Edmund, B. Webb, J.A. Zimmerman, and S.C. Seel: Reconsideration of continuum thermomechanical quantities in atomic scale simulations. *Math. Mech. Solids* **13**, 221 (2008).
82. K. Esfarjani, J. Garg, and G. Chen: *Modeling Heat Conduction from First Principles* (Annual Review of Heat Transfer, 2014), p. 9.
83. D.G. Cahill, P.V. Braun, G. Chen, D.R. Clarke, S. Fan, K.E. Goodson, P. Keblinski, W.P. King, G.D. Mahan, A. Majumdar, H.J. Maris, S. R. Phillpot, E. Pop, and L. Shi: Nanoscale thermal transport. II. 2003–2012. *Appl. Phys. Rev.* **1**, 011305 (2014).

https://doi.org/10.1557/mrc.2017.116 Published online by Cambridge University Press